

Reaction Engineering of Cocondensing (Methyl)ethoxysilane Mixtures: Kinetic Characterization and Modeling

Stephen E. Rankin[†] and Alon V. McCormick*

University of Minnesota, Department of Chemical Engineering and Materials Science,
421 Washington Avenue SE, Minneapolis, Minnesota 55455

Received March 20, 2000; Revised Manuscript Received August 18, 2000

ABSTRACT: Molecular homogeneity frequently plays a decisive role in the effective application of organically modified silicate copolymers, but direct characterization methods are not always available or convenient. We present an alternative tool for determining kinetic parameters for alkoxysilane hydrolytic copolycondensation using a semibatch reactor with varying time of injection of one component. All necessary kinetic parameters are determined from a series of ordinary ^{29}Si NMR data in a straightforward case study: copolymerization of dimethyldiethoxysilane and trimethylethoxysilane. As further validation of the rate coefficients, the results of a new series of experiments (varying the monomer ratio) are successfully predicted by the semibatch copolymerization model. With this model, we explore optimizing the molecular homogeneity of the copolymer products. Even for this relatively simple system, the optimal injection time is a complex function of residence time, but early injection of the faster-condensing monomer gives the best homogeneity at long residence times.

Introduction

Many low-organic content siloxanes which resemble ceramics but display novel properties have recently been synthesized from alkoxysilanes.¹ Examples include, but are far from limited to, novel optical materials, hard coatings,² modified disordered³ and hexagonally ordered⁴ porous materials, ambient-pressure aerogels,⁵ biological encapsulants,⁶ and modified bioactive ceramics.⁷ This paper will describe a new approach to characterizing, with the goal of controlling, the hydrolytic copolycondensation of mixed silicon alkoxide systems.

To optimize these organically modified silicates, we would like to control the extent of cocondensation between sites of differing extent or type of organic substitution. This distribution strongly influences the copolymer's properties, including thermal and chemical stability, surface properties, chemical properties, and, presumably, the self-assembly of the copolymers. Molecular homogeneity is not trivial to characterize, however. The best direct method of characterizing site homogeneity in *organic* copolymers, ^1H nuclear magnetic resonance (NMR), does not work well for siloxanes; the protons in the organic groups attached to the silicon sites (such as $\text{H}_3\text{C}-\text{Si}$) are too far removed from the polymer backbone to provide a strong chemical shift signature of molecular homogeneity. Instead, many investigators have found chemical shift signatures of cocondensation in NMR spectra of nuclei which make up the siloxane backbone— ^{17}O and ^{29}Si .

Babonneau and co-workers have reported clear ^{17}O chemical shift signatures of cocondensation between pairs of methylethoxysilanes⁸ and have even followed the evolution of cocondensing alkoxysilanes in situ.⁹ The technique has some disadvantages, however: broad

peaks from oxygen nuclei in different environments frequently overlap,¹⁰ and expensive ^{17}O enrichment is needed (the natural abundance of this isotope is low). The former problem cannot be easily overcome because fast spin polarization relaxation of the ^{17}O nucleus itself causes the broadening.¹¹

By working at low hydrolysis extents, ^{29}Si NMR peaks from homo- and heterocondensate dimers were identified in cocondensing mixtures of tetraethoxysilane (TEOS) and methyl- (MTEOS), ethyl-, or phenyltriethoxysilane^{11,12} or dimethyldiethoxysilane.¹³ The chemical shift difference between these dimers is small, however, and in larger oligomers produced by alkoxysilane polymerization, the peaks from heterocondensates and homocondensates are actually broad collections of peaks from a distribution of structures. These peaks may overlap significantly, making quantification difficult.^{14,15} More complex 2-dimensional NMR techniques¹⁶ are available to characterize molecular homogeneity through ^{29}Si – ^{29}Si correlations, but they take too long for kinetic investigations.

To investigate condensation kinetics, it has been widely assumed that characterization of molecular homogeneity is the limiting factor. Therefore, most studies have been limited to low water content so that only small oligomers (at most dimers or trimers) are present and can clearly be assigned. Prabakar and Assink,^{10,17} for the methyltriethoxysilane ($^{\text{MeT}}$)/TEOS (Q) system, compared dimerization kinetics of ($^{\text{MeT}} + ^{\text{MeT}}$), (Q + Q), and ($^{\text{MeT}} + \text{Q}$) reactions using ^{29}Si NMR. We¹⁸ have also compared homocondensation and heterocondensation by ^{29}Si NMR in a simpler mono- plus difunctional system but are still looking at a composition where the number of species formed is small. However, the evolution of easily measured global quantities (such as the connectivity distribution) is sensitive to the composition of the reacting system because of copolymerization. We have previously hypothesized that this sensitivity should be sufficient to allow one to distinguish homo- and cocondensation pathways in an alkoxysilane mixture.¹⁹

* Corresponding author. Telephone: 612-625-1822. Fax: 612-626-7246. E-mail: mccormic@cems.umn.edu.

[†] Current address: University of Kentucky, Chemical and Materials Engineering Department, 177 Anderson Hall, Lexington, KY 40506.

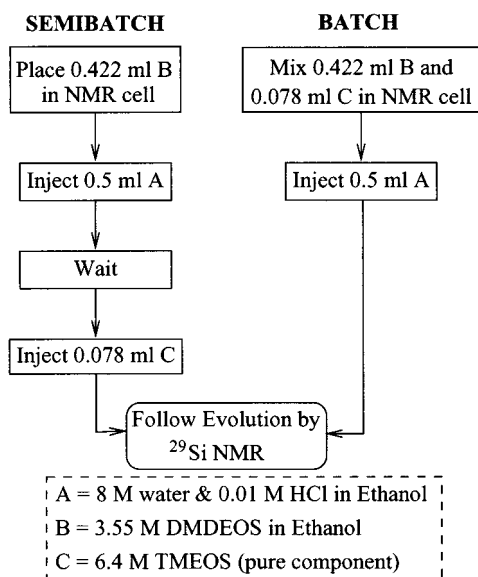


Figure 1. Flowsheet of sample preparation procedure. At the left, semibatch samples are prepared by first hydrolyzing the difunctional monomer (DMDEOS), then injecting the monofunctional monomer (TMEOS). At the right, both monomers are present from the start.

Here we will test this hypothesis by using experimental design, rather than novel characterization techniques, to measure copolymerization kinetics of bicomponent alkoxy silane systems over a wide range of reaction extents and with *no* direct cocondensation measure. This characterization will be done using ordinary ^{29}Si NMR. Specifically, we will describe the use of a *semibatch* reactor to provide conditions such that the evolution of the overall connectivities of the sites in a series of experiments is sensitive to both homo- and heterocondensation. Although copolymerization will not be directly measured, we will determine all copolymerization rate coefficients on the basis of this series of experiments, will *predict* the outcome of a new series of semibatch experiments, and will comment on the molecular homogeneity of the copolymer products.

Experimental Methods

Samples were prepared with trimethylethoxysilane (TMEOS) (> 98%, Aldrich), dimethyldiethoxysilane (DMDEOS) (United Chemical Technologies), filtered deionized water (prepared in house), a 1 N hydrochloric acid solution (from Aldrich), and anhydrous grade ethanol (Aaper Alcohol & Chemical). Before preparing the samples, 1 wt % of chromium(III) acetylacetonate was added to the ethanol as a paramagnetic relaxation agent. $\text{Cr}(\text{acac})_3$ finds frequent use as a paramagnetic relaxation agent because it does not dissociate readily and does not bind strongly to solutes (minimizing chemical shift changes).²⁰ Also, $\text{Cr}(\text{acac})_3$ does not affect ethoxysilane hydrolytic polycondensation at our hydrochloric acid concentration.²¹

Figure 1 illustrates the procedure used to prepare the samples. The "semibatch" samples were prepared by first placing a solution of the difunctional monomer in ethanol (solution B) in a septum-capped 5 mm (o.d.) glass NMR cell. Into this was injected a solution containing water and HCl in ethanol (solution A). Before injecting the monofunctional monomer (solution C), the concentrations were $[\text{Si}] = 1.62 \text{ M}$, $[\text{H}_2\text{O}]_0$ (before reaction) = 4.33 M, and $[\text{HCl}] = 0.00542 \text{ M}$. After waiting a variable amount of time (t_{inj}), solution C was added. After this addition, samples were mixed rapidly by hand and the evolution of the system was followed by ^{29}Si nuclear magnetic resonance (NMR). The concentrations after addition of solution C were $[\text{Si}] = 2.0 \text{ M}$ (with $[\text{M}] = [\text{D}]/3$),

$[\text{H}_2\text{O}]_0$ (a fictitious value assuming no reaction) = 4.0 M, and $[\text{HCl}] = 0.005 \text{ M}$. We followed the evolution of samples with $t_{\text{inj}} = 1, 5, 10, 20, 40$, or 80 min. All reactions were carried out at room temperature ($21 \pm 0.2^\circ \text{C}$).

For the "batch sample", the procedure was the same but $t_{\text{inj}} = 0$ (and the initial conditions were the same as the fictitious initial conditions just specified after injecting solution C). To simplify the sample preparation, we added the monofunctional monomer to the difunctional monomer before adding the water solution (Figure 1). One other sample was studied by ^{29}Si NMR, which was of exactly the same composition as the others but without the monofunctional monomer being added (this is labeled "no M").

^{29}Si NMR spectra were collected using a Varian VXR-500 instrument with a broadband probe tuned to 99.3097 MHz. Quadrature detection was used. Ten seconds was allowed for relaxation between 12 μs (90°) ^{29}Si pulses, and inverse gated decoupling of protons at 500 MHz was used to minimize the possibility of a negative NOE. The interpulse delay was verified to be long enough to provide quantitative data by comparing spectra of a similar (but unreactive) sample collected with a 10 or 20 s interpulse delay. The only requirement for quantitative interpretation of NMR data is this check that the delay between pulses is long enough to allow all sites to relax sufficiently.²² The number of transients per spectrum was a compromise between the need for a large signal-to-noise ratio and rapid acquisition of spectra. This number was increased with time as the reaction slowed. An exponential line broadening factor of 1–3 Hz was applied to the raw NMR data before Fourier transformation to increase the signal-to-noise ratio.

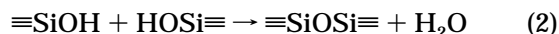
Results

NMR Spectra. Figure 2 shows a representative set of NMR spectra for this system. The displayed spectra are for the "batch" MD copolymerizing system—both monomers are present from the start. This experiment resembles that described previously,¹⁸ but with a lower M:D ratio, more water, and more HCl. From the first spectrum, there are several M_1 and D_1 peaks. The notation is as used elsewhere:²³ M denotes a monofunctional site, D a difunctional site, the subscript the number of siloxane bonds attached, and the superscript (if present) the number of hydroxyl groups attached. $\text{D}_{2,3c}$ and $\text{D}_{2,4c}$ are elements of rings containing three (hexamethylcyclotrisiloxane) or four (octamethylcyclotetrasiloxane) silicon sites, respectively.

As the system evolves, no obvious algebraic relationships between the peak intensities appear. This indicates that it is difficult or impossible to assign peaks to specific homo- or heterocondensation products. In fact, it seems that some of the peaks may be overlapping peaks from sites with differing second-shell environments. As one example, comparing (not shown) the intensities from different peaks it seems that $\text{M}_1 - \text{M}_1$ and $\text{M}_1 - \text{D}_1^1$ chemical shifts overlap. Unlike the previous simplified system,¹⁸ this precludes assignment and quantification of specific molecular species or even of the overall cocondensation extent for this system by ordinary 1D ^{29}Si NMR.

However, we can still assign peaks by their nearest neighbor environment (functionality and number of siloxyl and hydroxyl groups) easily. Following assignments in the chemical literature,^{16,23–25} Table 1 summarizes the chemical shift assignments we use. These assignments apply to all spectra in all data series.

Hydrolysis



As in previous work, we begin by examining hydrolysis

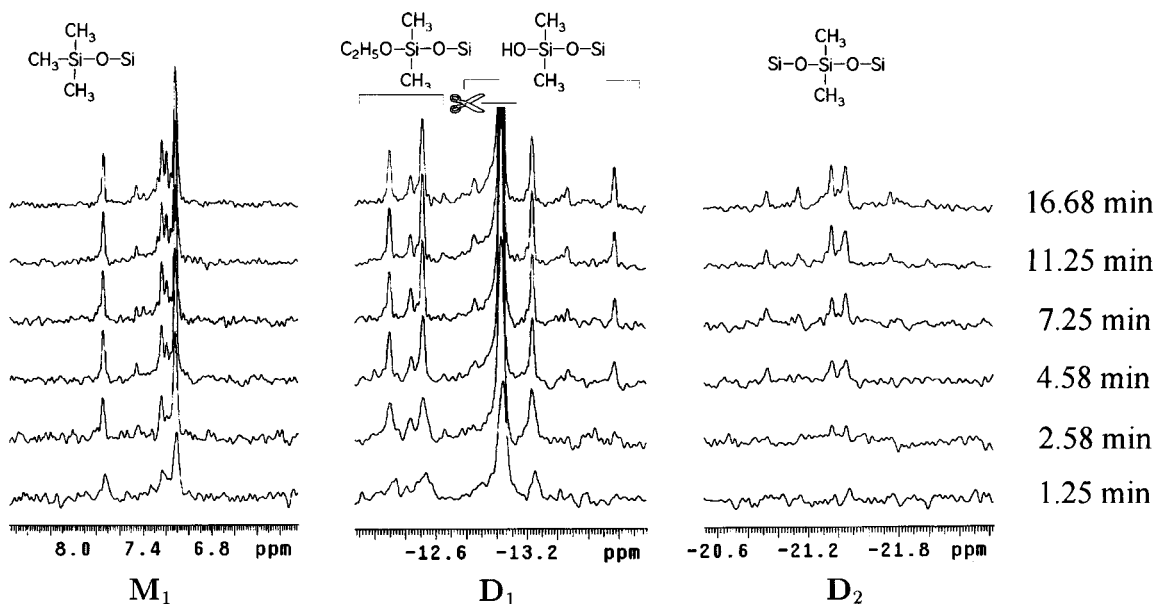


Figure 2. Representative sections of ^{29}Si NMR spectra for the copolymerizing system studied here. The types of sites are indicated below each section. The sample is the "batch" sample ($t_{\text{inj}} = 0$). Times are indicated to the right of each spectrum.

Table 1. Chemical Shift Assignments Used Here

site	chemical shift (ppm from $\text{Si}(\text{Me})_4$)
M_0^0	17.3
M_0^1	14.3
M_1	7.0 to 7.74
D_0^0	-3.7
D_0^1	-4.3
D_0^2	-4.8
$\text{D}_{2,3c}$	-8.5
D_0^1	-12.2 to -12.7
D_1^1	-12.8 to -13.8
$\text{D}_{2,4c}$	-18.9
D_2	-20.8 to -22.0

(eq 1) behavior. When fractional hydrolysis extents ($\chi_i^X = \sum_j j[X_j^i]/\sum_j [X_j^i]$) are plotted as a function of the condensation (eq 2) extent of the next-most condensed site, constant values are reached by the first measured point in all sites and all experiments (not shown). This tells us²⁶ that hydrolysis is reversible and fast enough to reach pseudoequilibrium. We can also see this pseudoequilibrium by following the apparent hydrolysis equilibrium coefficients using the definition

$$K_{h,i}^{X,\text{app}} = \frac{(\sum_j j[X_j^i])[\text{EtOH}]}{(\sum_j (f-i-j)[X_j^i])[\text{H}_2\text{O}]} \quad (3)$$

where

$$[\text{EtOH}] = [\text{EtOH}]_0 \frac{V_0}{V} + \sum_{X=M,D} \sum_{f=0}^f \sum_{j=0}^{f-i} (i+j)[X_j^i] \quad (4)$$

$$[\text{H}_2\text{O}] = [\text{H}_2\text{O}]_0 \frac{V_0}{V} - \sum_{X=M,D} \sum_{f=0}^f \sum_{j=0}^{f-i} \left(\frac{1}{2}i+j\right)[X_j^i] \quad (5)$$

and f is the functionality of monomer X .

Figure 3 shows that when the apparent hydrolysis equilibrium coefficient for sites of connectivity i is plotted as a function of the concentration of the next-most-connected site ($[X_{(i+1)}]$), all data are randomly scattered about an average value of 18 (the scatter

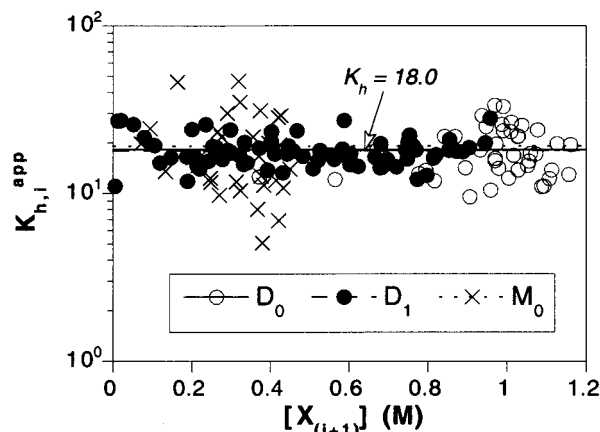


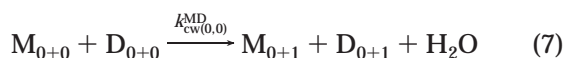
Figure 3. Apparent hydrolysis equilibrium coefficients of all sites as a function of the concentration of that site's condensation product. Points are from ^{29}Si NMR data and the lines are the average values (all $K_h = 18$). All eight time-series data sets are plotted.

comes from the low concentrations of some sites used to determine the coefficients). That the $K_{h,i}^{X,\text{app}}$ values are constant tells us that the actual hydrolysis equilibrium state has been reached and is maintained throughout. Because the equilibrium coefficient is the same for all sites, hydrolysis is random with an actual equilibrium coefficient of $K_h = 18 \times 10^{\pm 0.25}$. (By random, we mean that uncondensed groups on all sites are equally likely to be hydrolyzed.) This value is consistent with hydrolysis equilibrium coefficients measured for monofunctional²⁷ and difunctional²⁸ systems. Note that the scatter in the data is lowest for the D_1 sites, because they are present at highest concentration over the represented interval.

That hydrolysis is fast and equivalent for all sites is a major advantage for studying this cocondensation system. Previous investigations of alkoxy-silane copolymerization^{29,30} focused primarily on differences in hydrolysis rate (perhaps because these rates are easiest to measure by following monomer decay). For the samples studied here and other acid-catalyzed alkoxy-silanes, differences in hydrolysis rate become irrele-

vant²⁶—both from the standpoint of experimental characterization of polymerization kinetics and from the standpoint of the influence of hydrolysis kinetics on structure development. For the rest of this paper, we will focus on relative condensation and cocondensation kinetics for this system.

Semibatch Cocondensation Modeling. In previous reports on alkoxysilane copolymerization kinetics,^{17,18} investigators could measure cocondensation extent, for instance, the concentration of M sites attached to an M site (M_{1+0}) vs a D site (M_{0+1}). (X_{a+b} represents a site with a siloxane bonds to the same type of site and with b siloxane bonds to the other component.) Therefore, we could distinguish between, for instance, a reaction between two M_0 sites (eq 6) and a reaction between an M_0 and a D_0 site (eq 7) from a single kinetic experiment.



Here, we do not have the luxury of distinguishing both types of M_1 sites and must proceed with only information about the *total* number of siloxanes at each site (i.e., with $[M_1] = [M_{1+0}] + [M_{0+1}]$). To do so, we provide the M_0 site with an environment containing variable amounts of other M_0 sites, D_0 sites, and D_1 sites and watch how the monomer consumption changes. If our condensation model properly accounts for the rate dependence of each of the condensation reactions of the monomer, then we should be able to determine all three rate coefficients responsible for monomer consumption by fitting the model to the entire set of data.

By analogy with free-radical copolymerization kinetics,³¹ we could simply vary the monomer ratio in a series of batch experiments. While we showed in a preliminary communication that the phase portrait of this system changes qualitatively in this series of experiments,¹⁹ this is not the best approach to determine all cocondensation rate coefficients. The reason is that the monomers are always present together from the start of the reaction. Because of this, primarily the competition between cocondensation and homocondensation of the *monomers* determines the evolution of the system. The evolution is insensitive to the rate of reaction of the M monomer with D chain ends, so we cannot determine $k_{cw(0,0)}^{MD}$ well using this approach.

A better approach is to keep the ratio between monomers the same but to perform semibatch experiments (see Figure 1). The slower-reacting (D) monomer is allowed to react for certain lengths of time before the faster-reacting (M) monomer is injected. Because the set of D sites present at each injection time is different, this allows us to monitor reactions of the M monomer with both D monomers and D chain ends (D_1 sites). Therefore, we took this approach (as described in the Experimental Section).

Before,¹⁸ we modeled alkoxysilane copolymerization in a batch reactor with three main kinetic features: hydrolysis pseudoequilibrium, first-shell substitution effects for condensation, and cyclization to make three- and four-silicon rings.²⁸ We kept those kinetic features but modified the model to account for initially isolating one reactant from the mixture and adding it at an arbitrary point.

There are two primary effects of semibatch reactor operation compared to batch reactor operation. One, obviously, is that of adding the material itself. The other is the increase in the total volume of the system (dilution). These effects result in equations for each component of the form:

$$\frac{d[X_i]}{dt} = (\text{reaction terms}) + \frac{[X_i]_{inj} V_{inj} \Gamma(t)}{V(t)} - \frac{[X_i] V_{inj} \Gamma(t)}{V(t)} \quad (8)$$

addition
dilution

where $[X_i]_{inj}$ is the concentration of component X_i in the solution which is injected at time t_{inj} , V_{inj} is the volume of solution injected, the volume (V) varies with time according to eq 9, and Γ defines the rate of addition of material. For the "pulsed semibatch" reactor experiments conducted here, we use a Gaussian function for Γ centered at t_{inj} (the injection time) of width $\sigma = 15$ s (eq 10). The integrated results are not strongly dependent on σ as long as it is reasonably small.

$$\frac{dV}{dt} = V_{inj} \Gamma(t) \quad \text{where} \quad \int_0^\infty \Gamma(t) dt = 1 \quad (9)$$

$$\Gamma(t) = \frac{1}{\sqrt{2\pi}\sigma} \exp\left\{-\frac{1}{2}\left(\frac{t_{inj} - t}{\sigma}\right)^2\right\} \quad (10)$$

Naturally, dilution affects reaction rates through their explicit dependence on reactant concentrations. A secondary effect is that of diluting the *catalyst*, hydrochloric acid. All reaction terms should be affected the same way by this, though. Assuming straightforward acid catalysis, we assume the order with respect to $[HCl]$ to be one for all condensation reactions (this assumption has been verified for the monofunctional system³²). Then eq 8 becomes

$$\frac{d[X_i]}{dt} = (\text{reaction terms}) \frac{[HCl]}{[HCl]_0} + \frac{[X_i]_{inj} V_{inj} \Gamma(t)}{V} - \frac{[X_i] V_{inj} \Gamma(t)}{V} \quad (11)$$

Since HCl is neither produced nor consumed by reaction, $[HCl] = [HCl]_0 V_0/V$ where V_0 is the initial volume of the reactive solution, so eq 11 can be rewritten in terms only of volumes:

$$\frac{d[X_i]}{dt} = (\text{reaction terms}) \frac{V_0}{V(t)} + ([X_i]_{inj} - [X_i]) \frac{V_{inj} \Gamma(t)}{V(t)} \quad (12)$$

The resulting set of coupled differential equations for a semibatch reactor where M monomer is the only component added after the initial mixing is presented below (equation set 13) where we do not differentiate between the number of homolinkages and heterolinkages between sites. In this set of equations, all condensation reactions are assumed to be irreversible (consistent with previous kinetic modeling of homocondensation of alkoxysilanes²³).

$$\begin{aligned}
\frac{d[M_0]}{dt} &= -\hat{C}_0^M[M_0]\frac{V_0}{V(t)} + \{[M_0]_{\text{inj}} - [M_0]\}\frac{V_{\text{inj}}}{V(t)}\Gamma(t) \\
\frac{d[M_1]}{dt} &= -\hat{C}_0^M[M_0]\frac{V_0}{V(t)} - [M_1]\frac{V_{\text{inj}}}{V(t)}\Gamma(t) \\
\frac{d[D_0]}{dt} &= -\hat{C}_0^D[D_0]\frac{V_0}{V(t)} - [D_0]\frac{V_{\text{inj}}}{V(t)}\Gamma(t) \\
\frac{d[D_1]}{dt} &= \{\hat{C}_0^D[D_0] - \hat{C}_1^D[D_1] - 2\overline{k_{\text{eff}(3c)}}[L_3] - \\
&\quad 2\overline{k_{\text{eff}(4c)}}[L_4]\}\frac{V_0}{V(t)} - [D_1]\frac{V_{\text{inj}}}{V(t)}\Gamma(t) \\
\frac{d[D_2]}{dt} &= \{\hat{C}_1^D[D_1] - \overline{k_{\text{eff}(3c)}}[L_3] - 2\overline{k_{\text{eff}(4c)}}[L_4]\}\frac{V_0}{V(t)} - \\
&\quad [D_2]\frac{V_{\text{inj}}}{V(t)}\Gamma(t) \\
\frac{d[D_{2,3c}]}{dt} &= 3\overline{k_{\text{eff}(3c)}}[L_3]\frac{V_0}{V(t)} - [D_{2,3c}]\frac{V_{\text{inj}}}{V(t)}\Gamma(t) \\
\frac{d[D_{2,4c}]}{dt} &= 4\overline{k_{\text{eff}(4c)}}[L_4]\frac{V_0}{V(t)} - [D_{2,4c}]\frac{V_{\text{inj}}}{V(t)}\Gamma(t) \\
\frac{d[L_2]}{dt} &= \{2\overline{k_{\text{eff}(0,0)}}[D_0]^2 - 2\hat{C}_1^D[L_2]\}\frac{V_0}{V(t)} - [L_2]\frac{V_{\text{inj}}}{V(t)}\Gamma(t) \\
\frac{d[L_3]}{dt} &= \{4\overline{k_{\text{eff}(0,1)}}[L_2][D_0] - 2\hat{C}_1^D[L_3] - \\
&\quad \overline{k_{\text{eff}(3c)}}[L_3]\}\frac{V_0}{V(t)} - [L_3]\frac{V_{\text{inj}}}{V(t)}\Gamma(t) \\
\frac{d[L_4]}{dt} &= \{4\overline{k_{\text{eff}(0,1)}}[L_3][D_0] + 2\overline{k_{\text{eff}(1,1)}}[L_2]^2 - 2\hat{C}_1^D[L_4] - \\
&\quad \overline{k_{\text{eff}(4c)}}[L_4]\}\frac{V_0}{V(t)} - [L_4]\frac{V_{\text{inj}}}{V(t)}\Gamma(t) \\
\frac{dV}{dt} &= V_{\text{inj}}\Gamma(t) \quad (13)
\end{aligned}$$

where

$$\begin{aligned}
\hat{C}_0^M &= \overline{k_{\text{eff}(0,0)}^M}[M_0] + \sum_{i=0}^1 \overline{k_{\text{eff}(0,i)}^{\text{MD}}}(2-i)[D_i] \\
\hat{C}_i^D &= \overline{k_{\text{eff}(0,i)}^{\text{MD}}}(2-i)[M_0] + \sum_{i=0}^1 \overline{k_{\text{eff}(i,i)}^D}(2-i)(2-i)[D_i] \\
\overline{k_{\text{eff}(0,0)}^M} &= \chi_0^{M^2} k_{\text{cw}(0,0)}^M + \chi_0^M(1-\chi_0^M)k_{\text{ca}(0,0)}^M \\
\overline{k_{\text{eff}(i,i)}^D} &= \chi_i^D \chi_i^D k_{\text{cw}(i,i)}^D + \chi_i^D(1-\chi_i^D)k_{\text{ca}(i,i)}^D + \\
&\quad (1-\delta_{ii})\chi_i^D(1-\chi_i^D)k_{\text{ca}(i,i)}^D \\
\overline{k_{\text{eff}(0,i)}^{\text{MD}}} &= \chi_0^M \chi_i^D k_{\text{cw}(0,i)}^{\text{MD}} + \chi_0^M(1-\chi_i^D)k_{\text{ca}(0,i)}^{\text{MD}} + \\
&\quad \chi_i^D(1-\chi_0^M)k_{\text{ca}(i,0)}^{\text{DM}} \\
\delta_{ii} &= \text{Kronecker delta}
\end{aligned}$$

L_j = linear oligomer made up of j difunctional sites

While fitting, we neglected alcohol-producing condensation,^{32,33} so that the effective condensation rate coef-

ficients can be written as the product of two hydrolysis extents and the appropriate water-producing condensation rate coefficient. To determine the hydrolysis extent, we use the evidence (see above) that all hydrolysis equilibrium coefficients are equal ($K_h = 18$) and simply solve eq 3 to get

$$\chi_0^M = \chi_0^D = \chi_1^D = \frac{-b - \sqrt{b^2 - 4ac}}{2a} \quad (14)$$

where

$$\begin{aligned}
a &= (K_h - 1)(1 - \alpha) \\
b &= -(E + \alpha + K_h(W + 1 - 1.5\alpha)) \\
c &= K_h(W - \alpha/2) \\
W &= [H_2O]/([M] + 2[D]) \\
E &= [EtOH]/([M] + 2[D]) \\
\alpha &= \frac{[M_1] + [D_1] + 2([D_2] + [D_{2,3c}] + [D_{2,4c}])}{[M] + 2[D]}
\end{aligned}$$

Equations 4 and 5 are used to calculate $[EtOH]$ and $[H_2O]$, respectively.

Cocondensation Kinetics. Figure 4 shows the integrated ²⁹Si NMR results for all eight experiments performed. The data are shown as points and the best-fit numerical solution of equation set 13 as solid curves. The equations were solved with an Adams–Moulton method (a predictor–corrector method with fixed step size³⁴) and minimization of the residual function (the sum of squares of differences between the calculations and data) was accomplished with a Levenberg–Marquardt algorithm³⁵ (a hybrid steepest-descent/Newton–Raphson method suitable for multidimensional nonlinear least-squares problems). One set of coefficients was used to match all eight experiments. The reported values were found using several different initial guesses of the parameter values.

Figure 4 demonstrates that our model contains sufficient detail to match the experimental trends. The rate coefficients found by this fitting, along with the condensation scheme used here, are presented in Figure 5. The uncertainty estimates on the coefficients (found by analysis of the linearized residual surface near the optimal set of coefficients³⁵) indicate that we can be reasonably confident in the values of almost all of the rate coefficients we have determined, which is also an indication that the fit presented in Figure 4 is more than just a superficial match.

Discussion

First, we compare the trends in condensation rate coefficients to those we and others have observed. The strong decrease in reactivity with increasing connectivity of the D sites is consistent with observations of homopolymerizing systems.²³ The order of magnitude of the rate coefficients also agrees very well with that previously reported when allowance for the activity of HCl is made (see below).

The cocondensation rate coefficients for D_0 and D_1 are intermediate between those of the corresponding homocondensation reactions and lie closer to the faster-reacting components. These observations are consistent with the trends observed in batch reactors for MD

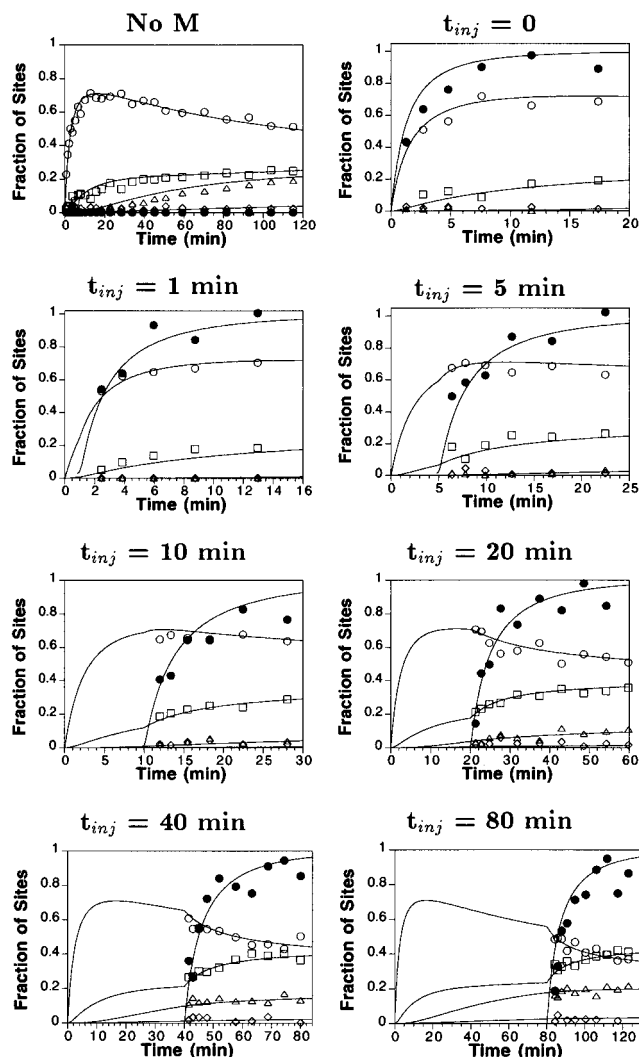
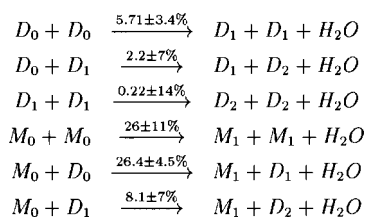


Figure 4. Fitting to experiments with variable injection time of the monofunctional component (t_{inj}). Points are data and curves are the best fit of the modeling equations (see text) to those data. One set of rate coefficients was used for all eight experiments shown here. Symbols denote D_1 (\circ), D_2 (\square), $D_{2,3c}$ (\diamond), $D_{2,4c}$ (\triangle), and M_1 (\bullet).

Bimolecular reactions (units of $l \cdot mol^{-1} \cdot hr^{-1}$)



Unimolecular reactions (units of hr^{-1})

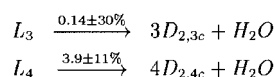


Figure 5. Cocondensation reaction scheme for the MD system, along with the water-producing condensation rate coefficients determined by least-squares fitting to the experimental data.

copolymerization¹⁸ and for MTEOS/TEOS dimerization.¹⁷ It is interesting, though, that the rate coefficient for condensation of M_0 with either M_0 or D_0 is about the same. Also, the rate coefficient for condensation between

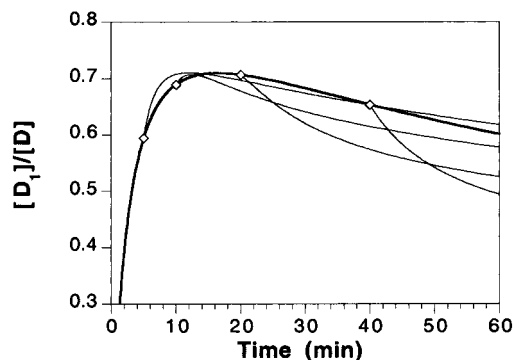


Figure 6. Calculated fractions of difunctional sites which are singly connected as a function of time. The thick line is calculated without monofunctional monomer present and the thin lines are calculated with the injection times indicated by open diamonds. Note that the y-axis range is expanded relative to Figure 4.

M_0 and a chain end (D_1) is still larger than that between two D_0 sites—emphasizing just how favorable “capping” reactions between M_0 sites and all D sites are.

As we mentioned in the modeling section, we chose our experiments to provide sensitivity not only to the monomer–monomer cocondensation rate coefficient but also to the $(M_0 + D_1)$ cocondensation rate coefficient. The small uncertainties in these coefficients in Figure 5 shows that this strategy worked, but as additional graphic evidence, Figure 6 presents the fraction of singly connected difunctional (D_1) sites as a function of time for varying t_{inj} . Shown are the calculated curves using the rate coefficients in Figure 5.

At low t_{inj} , D_1 sites are formed *more rapidly* than they are in the absence of the monofunctional monomer. This indicates that M_0 is reacting with the difunctional monomer to produce more D_1 than is produced by D_0 homocondensation. This change should be sensitive to $k_{cw(0,0)}^{MD}$. At later times (near the maximum in the unperturbed concentration of D_1) however, the rate of D_1 consumption increases because of the M monomer being added. For these t_{inj} values, the system's evolution is sensitive to $k_{cw(0,1)}^{MD}$. The sudden drop in the fraction of D_1 sites after M addition indicates that cocondensation between M_0 and D_1 sites is very favorable compared to homocondensation of D_1 sites, as long as conditions are chosen where the monofunctional monomer is present at the same time as the D_1 sites. This observation may be useful for preparing siloxanes of well-defined molecular weight (by “capping”).

Validation of Model Predictions. While the high quality of the fit in Figure 4 and the uncertainty analysis of the results demonstrate well enough that we have been able to quantify cocondensation kinetics without a direct measure of cocondensation, we will challenge our methodology even further by attempting to predict the outcome of a *new* set of experiments under different conditions. The new set of experiments is performed in the usual semibatch way by first mixing the difunctional monomer (0.5 mL of a 4.48 M DMDEOS solution in EtOH) with water and HCl (0.5 mL of a 9 M H_2O /0.0045 M HCl solution in EtOH), and after 30 min adding the monofunctional monomer. This time, however, the time of injection is kept constant and the amount of TMEOS injected is varied to give M:D ratios of 0, $1/4$, $1/2$, and 1. The experiments were conducted and analyzed exactly as the experiments in the rest of the text were.

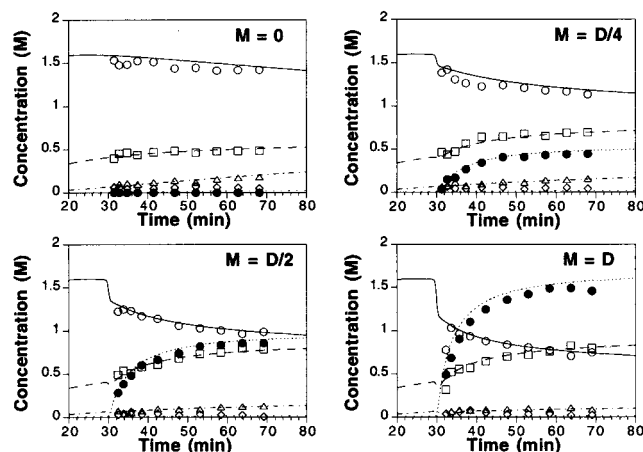


Figure 7. Comparison between predicted curves and experimental data (points) for the series a constant injection time of 30 min and variable M/D ratio. Symbols denote D_1 (○), D_2 (□), $D_{2,3c}$ (◇), $D_{2,4c}$ (△), and M_1 (●).

The conditions for this new series of experiments differ slightly from those of the series with varying t_{inj} (the t -series) because we chose a well-characterized difunctional system at its maximum concentration of D_1 sites at the time of M injection. The concentrations before adding M match those of an earlier homopolymerization experiment.²³ We still assume that the rate of all reactions is proportional to the activity of HCl, so all rate coefficients were multiplied by $([HCl]_0/[HCl]_{0,t-series}) = 0.413$.

Because the amount of water consumed varies considerably with the M:D ratio, we also consider the effect of water content on the HCl activity coefficient (γ_{HCl}). In mostly ethanol solutions, $\gamma_{HCl} \propto [H_2O]^{-1}$.³⁶ We have verified this relationship³² for HCl catalysis of TMEOS dimerization up to $[H_2O] \sim 2$ M. To account for the effect of water on HCl activity here, we multiplied each reaction rate in equation set 13 by $[H_2O]_{t-series}/[H_2O]$. The value of the water concentration in the t -series did not wander too far from the average value of $[H_2O]_{t-series} \sim 2.3$ M, so we use this in our prediction.

Figure 7 shows the evolution of concentrations of species in this variable M/D series (points), along with the concentrations predicted (curves) using eq 13 with the parameters in Figure 5 and corrections for the activity of HCl. Given that no further adjustments to the parameters were made, the agreement is quite remarkable. Some adjustments to the estimated parameters might be made, but overall the ability of the model to predict the outcome of this new set of experiments provides excellent validation of our semibatch cocondensation model and characterization approach.

Molecular Homogeneity. Now that we have verified our model and coefficients, we return to the set of t -series experiments to examine what was the molecular homogeneity of the copolymers. First, we recall that the set of rate coefficients we have determined allow us to write equations distinguishing copolymerization from homopolymerization (for instance, the concentration of D sites attached to one other D site— $[D_{1+0}]$ —vs the concentration of D sites attached to one M site— $[D_{0+1}]$). The equations are analogous to equation set 13, but with homopolymerization and copolymerization terms of the condensation operators (\hat{C}_i^x) separated (this splitting is illustrated elsewhere¹⁸).

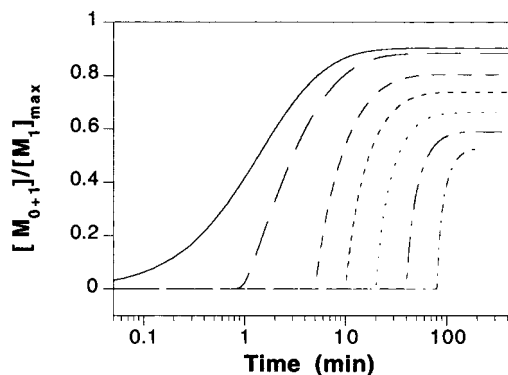


Figure 8. Calculated fraction of M_1 sites attached to D sites in a pulsed semibatch reactor as a function of time. Initial conditions are the same as the t -series experiments. Injection times are indicated by the point that the fraction starts to increase.

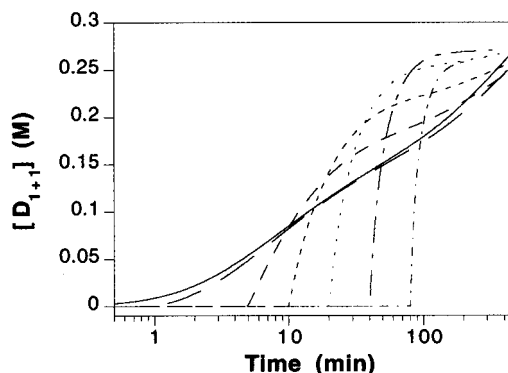


Figure 9. Calculated concentration of D_2 sites attached to one M site and to one D site in a pulsed semibatch reactor as a function of time. Initial conditions are the same as the t -series experiments. Injection times are indicated by the point that the concentration starts to increase.

Since M sites are the limiting reagent, the natural measure of molecular homogeneity is the fraction of M_1 sites attached to D sites. Figure 8 shows this quantity calculated under the conditions of the t -series experiments. Out of all of the t_{inj} values explored, the earliest injection clearly gives the highest level of molecular homogeneity at all times for this set of initial conditions. Early injection is so successful because the concentration of M monomers is always much smaller than the concentration of D sites. Because the rate coefficients for M homopolymerization and copolymerization with D_0 are very close, the best overall homogeneity is found when both monomers are present from the start.

What Figure 8 does not show is how many of the M sites end up on M–D–M trimers. While these trimers contain high number of M–D bonds, they leave the remaining D sites free to form high molecular weight oligomers containing no M sites. The M sites are more evenly distributed over the entire polymer population when they are located at the ends of longer polymer chains. A better indicator of the concentration of M sites terminating long chains is the concentration of D sites attached to one M site and to one D site ($[D_{1+1}]$).

Figure 9 shows this improved indicator of the M site homogeneity. Now the optimal injection time changes as the total residence time in the reactor changes. At very long residence times, early injection is still favorable. However, at short residence times, an intermediate injection time gives the best M site homogeneity. At those intermediate reaction times, M sites encounter

more D sites which have already reacted with one D site, so a high concentration of D_{1+1} sites develops quickly. Still, the rate of reaction of M site with D_1 sites is considerably lower than the rate of M homodimerization. Because M–M dimer formation competes with copolymerization, the advantage of using an intermediate injection time to improve overall homogeneity is short-lived. Eventually, the concentration of D_{1+1} sites that forms when M is present from the start meets or exceeds that observed with intermediate injection times.

Our cocondensation model can be used to more generally explore compositions and reactors giving siloxane copolymers with any desired structures. This exploration is beyond the scope of the present paper, however, so we conclude by reiterating that the homogeneity of these MD copolymers varies in a complex way during processing but that at long times, early addition of M monomers turns out to promote the most homogeneous structure. The conditions favoring this outcome are (1) the high rates of reaction of M monomers with anything else in the solution, relative to D homocondensation rates, and (2) the low M:D ratio. The strategy may be more complicated when relative hydrolysis rates interfere, especially when they contradict the condensation trend.

Conclusions

We have shown that cocondensation rate coefficients for bicomponent alkoxy silane systems can be determined from semibatch reactor studies. By performing a series of semibatch experiments where the time of injecting the more reactive monofunctional monomer changes, we have provided conditions to measure the rate at which trimethylsilanol reacts with itself, with hydrolyzed dimethyldiethoxysilane monomers, and with silanols at the end of difunctional dimers and chains.

Fitting the modeling equations with a single set of rate coefficients to this entire series of data, we have determined with fair to good confidence the complete set of homocondensation and cocondensation rate coefficients for the trimethylethoxysilane/dimethyldiethoxysilane system. Under the chosen conditions, these coefficients are *not measurable* by a single batch kinetic experiment without more elaborate spectroscopic techniques (giving the cocondensation extent).

The coefficients found were also used to predict the result of a similar series of experiments, this time varying the M:D ratio rather than the time of injecting the monofunctional reagent. The predictions of the model are quite good and match the NMR data nearly as well as they would if they were fit to those data. This demonstrates that we have developed a technique which not only characterizes but also *predicts* the evolution (and therefore the homogeneity as well) of bicomponent alkoxy silane systems.

Finally, the rate coefficients from the model were used to calculate the homogeneity of the copolymers present during the injection time series of experiments. The calculated homogeneity is a complex function of injection time and overall residence time in the reactor, but of all the pulsed semibatch reactor conditions explored here, the ones with the earliest injection times give the most homogeneous copolymers. Early injection should give the most molecularly homogeneous copolymer when (1) one component reacts much more quickly with itself and with the other component than the other component reacts with itself and (2) the ratio of the more reactive component to the less reactive component is low.

Acknowledgment. The authors thank the National Science Foundation and the University of Minnesota Graduate School (for graduate fellowships to S.E.R.), the NSF Center for Interfacial Engineering at the University of Minnesota, the Minnesota Supercomputer Institute, and Dow Corning Corporation for research funding and resources contributing to this work. We also thank Dr. Gary Wieber of Dow Corning for helpful discussions of this work.

References and Notes

- (1) Sanchez, C.; Ribot, F. *New J. Chem.* **1994**, *18*, 1007.
- (2) Schmidt, H. *Ceram. Trans.* **1995**, *55*, 253.
- (3) Schmidt, H.; Böttner, H. *Adv. Chem.* **1994**, *234*, 419.
- (4) Babonneau, F.; Leite, L.; Fontlupt, S. *J. Mater. Chem.* **1999**, *9*, 175.
- (5) Prakash, S. S.; Brinker, C. J.; Hurd, A. J. *J. Non-Cryst. Solids* **1995**, *190*, 264.
- (6) Inama, L.; Diré, S.; Carturan, G.; Cavazza, A. *J. Biotechnol.* **1993**, *30*, 197.
- (7) Tsuru, K.; Ohtsuki, C.; Osaka, A.; Iwamoto, T.; Mackenzie, J. D. *J. Mater. Sci. Mater. Med.* **1997**, *8*, 157.
- (8) Babonneau, F.; Maquet, J.; Livage, J. *Chem. Mater.* **1995**, *7*, 1050.
- (9) Babonneau, F.; Gualandris, V.; Pauthe, M. *Mater. Res. Soc. Symp. Proc.* **1996**, *435*, 119.
- (10) Prabakar, S.; Assink, R. A. *Mater. Res. Soc. Symp. Proc.* **1996**, *435*, 345.
- (11) Prabakar, S.; Assink, R. A.; Raman, N. K.; Myers, S. A.; Brinker, C. J. *J. Non-Cryst. Solids* **1996**, *202*, 53.
- (12) Sugahara, Y.; Inoue, T.; Kuroda, K. *J. Mater. Chem.* **1997**, *7*, 53.
- (13) Brus, J.; Dybal, J. *Polymer* **1999**, *40*, 6933.
- (14) Babonneau, F. *Polyhedron* **1994**, *13*, 1123.
- (15) Babonneau, F. *New J. Chem.* **1994**, *18*, 1065.
- (16) Lux, P.; Brunet, F.; Virlet, J.; Cabane, B. *Magn. Reson. Chem.* **1996**, *34*, 173.
- (17) Prabakar, S.; Assink, R. A. *J. Non-Cryst. Solids* **1997**, *211*, 39.
- (18) Rankin, S. E.; Macosko, C. W.; McCormick, A. V. *J. Polym. Sci. A* **1997**, *35*, 1293.
- (19) Rankin, S. E.; Macosko, C. W.; McCormick, A. V. *Mater. Res. Soc. Symp. Proc.* **1996**, *435*, 113.
- (20) Harris, R. K. *Nuclear Magnetic Resonance Spectroscopy. A Physico-Chemical View*; Wiley: New York, 1986.
- (21) Sanchez, J.; McCormick, A. V. *J. Phys. Chem.* **1992**, *96*, 8973.
- (22) Rabenstein, D. L.; Keire, D. A. *Quantitative Chemical Analysis by NMR. In Modern NMR Techniques and Their Application in Chemistry*; Popov, A. I., Hallenga, K., Eds.; Marcel Dekker: New York, 1991.
- (23) Rankin, S. E.; Macosko, C. W.; McCormick, A. V. *AIChE J.* **1998**, *44*, 1141.
- (24) Sugahara, Y.; Okada, S.; Kuroda, K.; Kato, C. *J. Non-Cryst. Solids* **1992**, *139*, 25.
- (25) Hook, R. J. *J. Non-Cryst. Solids* **1996**, *192*, 1.
- (26) Rankin, S. E.; McCormick, A. V. *Chem. Eng. Sci.* **2000**, *55*, 1955.
- (27) Šefčík, J.; Rankin, S. E.; Kirchner, S. J.; McCormick, A. V. *J. Non-Cryst. Solids* **1999**, *258*, 187.
- (28) Rankin, S. E.; Šefčík, J.; McCormick, A. V. *Ind. Eng. Chem. Res.* **1999**, *38*, 3191 and references therein.
- (29) Schmidt, H.; Scholze, H.; Kaiser, A. *J. Non-Cryst. Solids* **1984**, *63*, 1.
- (30) Alam, T. M.; Assink, R. A.; Loy, D. A. *Chem. Mater.* **1996**, *8*, 2366.
- (31) Dotson, N. A.; Galván, R.; Laurence, R. L.; Tirrell, M. *Polymerization Process Modeling*; VCH: New York, 1996.
- (32) Rankin, S. E.; Šefčík, J.; McCormick, A. V. *J. Phys. Chem.* **1999**, *103*, 4233.
- (33) Assink, R. A.; Kay, B. D. *Colloids Surf. A* **1993**, *74*, 1.
- (34) Dahlquist, G.; Björck, A. *Numerical Methods*; Prentice Hall: Englewood Cliffs, NJ, 1974.
- (35) Bard, Y. *Nonlinear Parameter Estimation*; Academic: New York, 1974.
- (36) Tourky, A. R.; Abdel-Hamid, A. A.; Slim, I. Z. *Z. Phys. Chem. Leipzig* **1972**, *250*, 49.